

This material may be downloaded for personal use only. Any other use requires prior permission of the American Society of Civil Engineers. This material may be found at [https://ascelibrary.org/doi/10.1061/\(ASCE\)MT.1943-5533.0001478](https://ascelibrary.org/doi/10.1061/(ASCE)MT.1943-5533.0001478).

The following publication Leng, Z., & Yu, H. (2016). Novel method of coating titanium dioxide on to asphalt mixture based on the breath figure process for air-purifying purpose. Journal of Materials in Civil Engineering, 28(5), 04015188 is available at [http://dx.doi.org/10.1061/\(ASCE\)MT.1943-5533.0001478](http://dx.doi.org/10.1061/(ASCE)MT.1943-5533.0001478).

1 A Novel Method of Coating Titanium Dioxide onto Asphalt

2 Mixture Based on Breath Figure Process for Air-purifying

3 Purpose

4 Zhen Leng^{1*}, A.M. ASCE; Huayang Yu²

5
6 **Abstract:** Titanium dioxide (TiO₂) is a photocatalyst that has the capability of
7 accelerating the oxidation of nitrogen oxides (NO_x) and other pollutants under ultraviolet
8 (UV) radiation. A number of studies have been conducted on applying TiO₂ onto
9 pavement surface to purify exhaust emissions from vehicles. However, it remains a
10 challenging task to effectively coat TiO₂ to asphalt pavements to achieve durable air-
11 purifying performance. This study aims to develop an innovative method, based on breath
12 figure (BF) process and Pickering emulsion effect, to coat TiO₂ particles onto asphalt
13 pavement surfaces. With this method, asphalt binder with micro pores filled with TiO₂
14 particles can be coated to asphalt pavement surfaces. The micro porous structure of the
15 coating material helps to provide larger contact area between TiO₂ and UV, thus
16 enhancing NO_x degradation efficiency. Microscopic analysis on the coating material
17 prepared using the new method demonstrated that TiO₂ particles distributed well on the
18 pore walls of the coating material, indicating that UV can reach TiO₂ to activate the

¹ Assistant Professor, Department of Civil and Environmental Engineering, The Hong Kong Polytechnic University, Hung Hom, Kowloon, Hong Kong, zhen.leng@polyu.edu.hk

(*Corresponding Author)

² PhD Candidate, Department of Civil and Environmental Engineering, The Hong Kong Polytechnic University, Hung Hom, Kowloon, Hong Kong, 13900586r@connect.polyu.hk

19 photocatalytic process. The nitric oxides (NO) removal efficiencies of the asphalt mixture
20 specimens coated using this new method and the traditional water-solution based method
21 after various numbers of surface abrasions were also measured by a custom-designed
22 environmental test setup. It was found that this new coating method provided not only
23 better NO removal efficiency but also improved durability to maintain the degradation
24 efficiency after tire abrasion, compared to the traditional method.

25 **Author keywords:** Photocatalytic process, Coating material, Micro pores, Breath
26 Figure process, NO removal efficiency

27

28 **Introduction**

29 Emerging functional pavements have been extensively reported by recent studies
30 (Stempihar et al. 2012; Losa. et al. 2013; Ballari and Brouwers 2013). These pavements
31 provide not only smooth riding surfaces to vehicles, but also various additional functions,
32 such as mitigating traffic noise, decreasing road surface temperature, and degrading
33 harmful vehicle gases. Among these emerging pavements, the air-purifying pavement,
34 which helps alleviate pollution due to vehicle emission, has gained rapidly increasing
35 interest.

36 The main hazardous substance from vehicle emission is nitrogen oxides (NO_x),
37 which is also the major precursor of particulate matter (PM) 2.5, the representative air
38 pollutant of photo-chemical smog and haze (Atkinson 2000). Although various types of
39 gas-cleaning equipment have been installed to vehicles, the NO_x concentration in traffic
40 environment is still unsatisfying, especially in urban areas with high traffic densities. To
41 further improve the traffic environment, attempts have been made to build pavement
42 surfaces that have the function of degrading NO_x . So far, the most common and effective
43 technology is to add titanium dioxide (TiO_2) to road surface, since TiO_2 is able to
44 accelerate the photocatalytic activity of NO_x under ultraviolet (UV) radiation. Besides,
45 properties such as high-chemical stability, super-hydrophilicity, and relatively low cost
46 make TiO_2 an ideal photocatalytic purifier (Agrios and Pichat 2005) to be incorporated
47 into pavement materials. A number of studies have verified the feasibility of this
48 technology to decrease NO_x concentration (Chen and Liu 2010; Dylla. et al. 2010; Shen.
49 et al. 2012; Hassan. et al. 2011; Hassan. et al. 2012).

50 To add TiO₂ particles onto road surfaces, the simplest way is to apply a thin TiO₂
51 coating layer. In order to activate the photocatalytic process, the TiO₂ catalysts should
52 have direct contact with UV and pollutants. Previous studies have shown that TiO₂
53 coating layers worked well on concrete pavements, but not so successful on asphalt
54 pavements (Venturini and Bacchi 2009; Dylla et al. 2010; Shen et al. 2012). On one hand,
55 the pollution removal efficiency of asphalt pavements with TiO₂ coating was not so
56 satisfying. On the other hand, the ability of asphalt pavements with TiO₂ coating to
57 maintain NO_x removal efficiency was relatively poor. One of the possible contributing
58 factors to such phenomenon is the porosity of the coating layer (Li and Qian 2009). The
59 porous microstructure on the rigid pavement surface helps to provide larger interaction
60 area between TiO₂ and UV, leading to higher degradation efficiency. Moreover, TiO₂
61 particles inside the micro pores are not easily removed by tire actions, resulting in better
62 durability.

63 However, most urban roads in the world are surfaced with asphalt mixture. Thus,
64 it becomes very meaningful to enhance the performance and durability of TiO₂ coating on
65 asphalt pavements. The main objective of this study is to develop a novel TiO₂ coating
66 method, based on breath figure (BF) process, for asphalt pavements, which is able to
67 provide improved performance in terms of both pollution removal efficiency and
68 durability. To achieve this objective, the following tasks have been conducted by this
69 study:

- 70 • Prepare TiO₂ coating solution by using the novel method based on BF process;
- 71 • Conduct microscopic analysis on the coating material using Scanning Election
72 Microscopy (SEM) and Energy Dispersive X-ray Spectroscopy (EDX) to

- 73 evaluate the distribution of TiO₂ on the coating material;
- 74 • Assess the NO_x removal efficiency of the asphalt mixture specimens coated
- 75 with TiO₂ using the novel method;
- 76 • Assess the durability of the coating material by measuring the NO_x removal
- 77 efficiencies of the asphalt mixture specimens with TiO₂ coating after various
- 78 numbers of lab-simulated tire abrasions.

79 **Research Background**

80 ***Photocatalytic NO_x Oxidation***

81 The photocatalytic oxidation property of TiO₂ was discovered by Fujishima in 1972

82 (Fujishima and Honda 1972). This discovery marked the beginning of a new age of using

83 photocatalytic process for the purpose of self-cleaning.

84 It has been well demonstrated that both organic pollutants and oxides such as

85 nitric oxide (NO), nitrogen dioxide (NO₂), and sulfur monoxide (SO), can be oxidized by

86 TiO₂ under UV irradiation (Agrios and Picha 2005). The photocatalytic oxidation begins

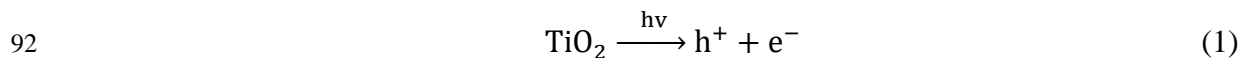
87 with the irradiation of light over TiO₂ particles. When TiO₂ absorbs a photon containing

88 the energy larger than or equal to its band gap, 3.2eV, an electron will be promoted from

89 the valence band to the conduction band, leaving a hole behind and creating electron-hole

90 pairs, which are also known as excitons (Zhao and Yang 2003; Chen and Poon 2009).

91 This process can be illustrated by Eq. 1.

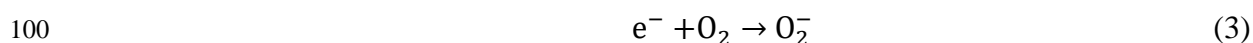
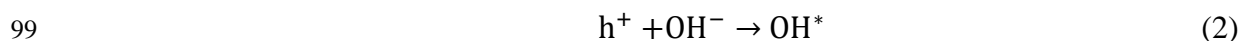


93 In the above reaction, h⁺ and e⁻ are powerful oxidizing and reducing agents,

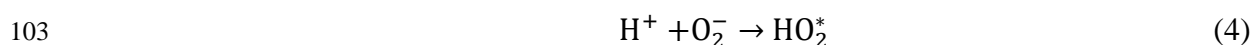
94 respectively. The strong oxidation power of h⁺ enables it to react with water to generate

95 the highly active hydroxyl radical (OH[•]), which is also a powerful oxidant. In addition,

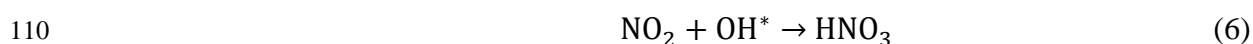
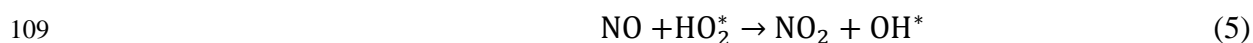
96 the power of the electrons can induce the reduction of molecular oxygen (O_2) to
 97 superoxide anion (O_2^-), which also has the strong capacity of degrading pollutants (Chen
 98 and Poon 2009). These two processes can be described by Eq. 2 and 3, respectively.



101 The superoxide anion can further react with H^+ dissociated from water to generate
 102 the HO_2^* radical, as Eq. 4 shows.



104 Most organic air pollutants can be degraded completely by either the OH^- or the
 105 holes themselves to innocuous final products. For example, NO can be oxidized to NO_2 ,
 106 and then both the hazardous gases (NO and NO_2) can be degraded to water soluble
 107 nitrates, as Eq.5 and 6 show (Agrios and Picha. 2005; Zhao and Yang 2003; Chen and
 108 Poon 2009; Dylla et al. 2014):



111 After the above reactions, the final product, nitric acid (HNO_3), can be easily
 112 washed away by rainwater.

113 It is worth noting that for the photocatalytic oxidation process described above,
 114 both TiO_2 and UV radiation are essential. As a result, it is necessary and important to
 115 provide enough contact area between TiO_2 particles and sunlight to ensure an efficient
 116 photocatalytic process.

117 ***Current Methods to Coat TiO_2 Particles onto Road Surfaces***

118 Various studies have been conducted on appropriate approaches to incorporate TiO₂
119 particles into pavement surfaces (Li and Qian. 2009; Hassan et al. 2011; Hassan et al.
120 2012; Ramirez et al. 2012; Shen et al. 2012). An ideal method should be able to provide
121 both high pollutant removal efficiency and good durability to maintain the efficiency
122 under vehicle tire abrasion.

123 Researchers from Louisiana tried various methods to coat TiO₂ onto concrete
124 pavement surface, including cement-water coating with TiO₂ and mineral fines, a
125 commercial product named PURETI, and directly spreading TiO₂ particles to fresh
126 concrete before curing (Dylla et al. 2010; Ramirez et al. 2012). It was reported that the
127 cement-water coating method performed the best, which achieved 26.9% and 20% NO
128 removal efficiency before and after abrasion, respectively, in a specific testing
129 environment. A study conducted at Washington State University investigated various
130 promising surface coating methods, such as cement/aggregate/TiO₂ mix (CATM), TiO₂
131 in water (TIW), and driveway protector mix (DPM), to apply TiO₂ coating to pervious
132 concrete pavement. The durability of the coating material was also measured by actual
133 weather exposure (Shen et al. 2012). It was found that the driveway protector mix (DPM)
134 treatment performed the best in pollution removal test and the sample with DPM
135 treatment also maintained a relatively high level of pollution removal efficiency after four
136 months of weathering.

137 Relatively few studies have been conducted to apply TiO₂ to asphalt pavements.
138 Venturini and Bacchi (2009) added TiO₂ particles into pervious asphalt pavements by
139 sprinkling water-based emulsion onto pavement surface. The NO_x reduction efficiency
140 was found between 20% and 57%, depending on the type of TiO₂ (rutile, anatase and

141 brookite), and anatase TiO₂ performed the best. After successfully applying TiO₂ onto
142 concrete pavements, the researchers from Louisiana further attempted applying water-
143 based TiO₂ spraying coating onto asphalt pavements (Hassan et al. 2011; Hassan et al.
144 2012). Satisfactory results were obtained when the TiO₂ coating was in the original state,
145 but it was also pointed out that the durability of TiO₂ coating required further study. Li
146 and Qian (2009) mixed TiO₂ particles with both cement concrete and asphalt mixture.
147 They found that the pollution removal efficiency of cement concrete was much better
148 than that of asphalt mixture. They believed that the porosity of concrete surface enabled
149 TiO₂ to be stored inside the surface pores, which made positive impact on both the NO
150 removal efficiency and the durability of air-purifying function.

151 It is worth noting that the NO_x removal performance of TiO₂ coating is dependent
152 on the area of TiO₂ exposed to sunlight and pollutants. A larger contact area between
153 TiO₂ and sunlight will provide better NO_x removal efficiency if all the other conditions
154 are the same. Previous studies have proved that the porous surface of cement concrete is a
155 potential factor that leads to the satisfied air-purifying performance of concrete
156 pavements (Dylla et al. 2010; Shen et al. 2012; Hassan et al. 2012; Li and Qian 2009;
157 Poon and Cheung 2007). To enhance the performance of air-purifying asphalt pavements,
158 it is very promising to fabricate highly ordered micro pores in asphalt pavement surfaces.
159 The micro pores can be achieved by various physical and chemical treatments, such as
160 lithography, colloidal crystal, and self-assembled block copolymers (Li et al. 2010).
161 Among these treatments, the one based on Breath Figure (BF) process has been
162 investigated in this study because it is relatively inexpensive and easy to implement
163 (Bunz 2006; Li et al. 2010).

164 ***Breath Figure Process***

165 BF process is essentially a common and unimpressive process that happens every day.
166 For example, the process of forming fog by breathing onto a cold surface is a BF process
167 (Bunz 2006). BF had long been considered as an annoying natural phenomenon till 1994,
168 when Widawski discovered the formation of an ordered porous film by casting a polymer
169 solution onto a substrate (Widawski et al. 1994). Since this discovery, the BF approach
170 has been developed into an amazing self-assembly strategy for the fabrication of porous
171 structures, with the pore sizes ranging from hundreds of nanometers to hundreds of
172 micrometers (Li et al. 2010).

173 In the BF process, the porous surface is achieved by water droplet condensation
174 during fast solvent evaporation under a humid flow. The mechanism of forming a porous
175 structure on a typical polymer surface can be described as follows: 1) the polymer is
176 dissolved in a low boiling point solvent, and then cast onto a solid substrate in a high-
177 humidity environment; 2) water droplets nucleate on the surface and grow subsequently
178 due to the evaporative cooling; 3) driven by the surface convection and capillary force,
179 the condensed water droplets self-assembles into hexagonal arrays; and 4) templated by
180 the formed droplet arrays, micro pores are formed on the polymer film surface as soon as
181 the solvent evaporates (Li et al. 2010).

182 In this study, BF process has been applied to build micro pores on the surface of
183 asphalt, which is essentially a type of polymer, to enlarge the contact area between the
184 sunlight and TiO₂ particles embedded into the micro pores and enhance the air-purifying
185 performance.

186 **Experimental Program**

187 ***Preparation of Coating Solution***

188 According to the mechanism of BF process, Tetrahydrofuran (THF) was selected as the
189 solvent of asphalt binder due to its ability to dissolve asphalt and its low boiling point
190 (66°C). The evaporation cooling effect of THF can decrease the solution surface
191 temperature and accelerate the condensation of vapor nearby quickly. SBS modified
192 asphalt with the performance grade of PG76-22 was selected as the coating binder.

193 During the trial experiment, it was found that the porous structure could not be
194 formed with THF and asphalt only. As asphalt has a low glass transition temperature, its
195 relatively high mobility makes the micro structure very easy to collapse, leading to
196 irregular bulking without micro pores on surface (Fig.1a). To solve this problem,
197 polystyrene (PS) was added to assist maintaining the formed microstructures. The
198 difference in micro feature between the samples with various PS-asphalt weight ratios
199 (total weight in THF: 60mg/ml) is shown in Fig.1. It can be seen that with the increase of
200 the amount of PS, more and more regular pore arrays can be observed. When the PS-
201 asphalt ratio reaches 10/10, clear honeycomb structure can be observed. Thus, the PS-
202 asphalt weight ratio of 10/10 was selected to prepare the porous TiO₂ coating solution.
203 The diameters of the micro pores as shown in Fig.1 d are approximately 10μm.

204 The coating solution was prepared under room temperature (20±3°C) and a
205 humidity of 60±5%. The porous coating (PC) solution with TiO₂ particles was prepared
206 by mixing all solutes, i.e., asphalt, PS and TiO₂ into certain amount of solvent (THF).
207 Two porous coating solutions with different weight ratios of TiO₂, asphalt, and PS, i.e.,
208 0.5/1/1 and 2/1/1, were prepared. The one with higher percentage of TiO₂ is labeled as H-

209 PC, while the one with lower percentage of TiO₂ is labeled as L-PC. Concentrations of all
210 solutes (including asphalt, PS and TiO₂) were 75mg/ml for L-PC and 120mg/ml for H-PC.

211 ***Substrate Preparation***

212 To measure the NO_x removal efficiency and durability of TiO₂ coating, standard Marshall
213 Specimens (diameter=101.6mm and height=63.5±2.5mm) were prepared as substrates to
214 simulate real asphalt pavement surfaces. The asphalt mixture used to prepare the
215 specimens was a gap-graded mixture with a design air void content of 4.4%. PG76-22
216 asphalt binder was used and the asphalt content was 6.1%. All substrate specimens were
217 compacted by a standard Marshall Compaction machine according to ASTM D6926.

218 L-PC and H-PC solutions were sprayed onto Marshall Specimen surfaces evenly
219 using a water sprayer. The spraying was conducted in a highly humid environment to
220 ensure the occurrence of the BF process. The dosage of both emulsions applied to each
221 Marshall specimen was 7ml. As a result, there were approximately 0.1g and 0.4g of TiO₂
222 on each specimen with L-PC and H-PC, respectively. To compare the NO_x removal
223 performance of the BF method with the traditional method, a water-based coating
224 solution (named as WC) was also prepared and applied. The dosage of TiO₂ coated on
225 each specimen using the traditional method was controlled at 0.4g, which is equal to that
226 of the specimen with H-PC. Table 1 shows the detailed information of the test specimens
227 for NO_x removal efficiency tests. For all groups except for OM, three replicate specimens
228 were prepared and tested to ensure the reliability of the test results (Fig. 2).

229 ***Micro Analysis***

230 For the purpose of microanalysis, L-PC and H-PC were dropped on both planar and non-
231 planar substrates. An opaque coating covering the substrates formed after the evaporation

232 of solvent. SEM JSM-6490 with EDX detector manufactured by JEOL Inc., US, was
233 employed to evaluate the morphology of the coating surface. Before observation, a thin
234 layer of gold was pumped onto the samples to obtain clear and reliable images.

235 ***NO_x Removal Efficiency Test***

236 A custom-designed environmental test setup was used to evaluate the NO_x removal
237 efficiency of the test specimens. The test system mainly consists of NO_x and zero air
238 cylinders, a reacting chamber, light source (UV lights), a NO_x data analyzer, and a data
239 recorder. Fig. 3a is a diagram of environmental test system, and Fig. 3b shows the
240 specimen inside reacting chamber during the testing process.

241 The reacting chamber is equipped with air inlet and outlet so that continuous flow
242 stream inside chamber can be maintained. The cover of the chamber was fabricated of
243 transparent glass rimmed with stainless steel, which allows UV light to reach the testing
244 specimen surface. Two fluorescent lamps were placed upon the chamber and their
245 distance to the chamber was adjusted till the required intensity was achieved (in this
246 study, the UV intensity was set as 10 W/m²). The wavelength of the UV light emitted
247 from fluorescent lamps was 365nm, which is very close to that of the UV from sunlight.
248 The temperature and humidity inside the reacting chamber were controlled at 20°C and
249 10%, respectively.

250 The NO_x data analyzer was able to record the amount of both NO and NO₂. In this
251 study, as the concentration of NO₂ remained a low level (<50ppb) during all tests, the
252 photocatalytic ability of the specimens was characterized by NO removal rate. At the
253 beginning of test, the gas streams were adjusted by the flow controllers to obtain the
254 initial NO concentration (X_{initial}), which is approximately 1200 ppb, and a flow rate of

255 3L/min inside the chamber. After around 30 minutes, the NO concentration inside the
256 chamber reached equilibrium, and then the degradation test was started by turning on the
257 UV lights. During the photocatalytic reaction, the concentration of NO was continuously
258 recorded by the analyzer. After another 30 minutes, the NO concentration (X_{stable}) in the
259 chamber reached another stable status. Based on the values of $X_{initial}$ and X_{stable} , the NO
260 removal rate (R%) can be calculated by Eq. 7. A higher NO removal rate indicates a
261 better pollutant removal efficiency.

$$262 \quad \% \text{ NO Removal Rate}(R\%) = \frac{X_{initial} - X_{stable}}{X_{initial}} \times 100\% \quad (7)$$

263 ***Durability Test***

264 Since the TiO₂ coating is vulnerable to tire abrasion, especially in wet condition, it is
265 necessary to evaluate the pollutant removal efficiency of TiO₂ coating not only in its
266 original state but also its ability to maintain the pollution removal function under tire
267 actions.

268 In this study, the British Pendulum Skid Resistance Tester was employed to
269 simulate tire abrasion. Before applying abrasion, the Marshall specimens with TiO₂
270 coating were first immersed in water for 3 minutes to produce the wet surface condition.
271 Then the Marshall specimen was fixed on ground, and the pendulum slider was
272 positioned barely in contact with the wet surface of the specimen according to ASTM
273 E303. The abrasion test was started by raising the pendulum to the lock position. Then
274 the pendulum was released, allowing the rubber slider to make contact with and pass by
275 the specimen surface. After the abrasion process was repeated for 50 and 200 times, the
276 NO_x removal ability was calculated by Eq. 8.

277
$$\% \text{ Residuary NO removal ability}(RA\%) = \frac{R_0 - R_x}{R_0} * 100\% \quad (8)$$

278 Where R_x is the NO removal rate after x times of abrasion and R_0 is the NO
279 removal rate when the TiO_2 coating is in the original state, i.e., without abrasion. A
280 higher residual rate indicates a better durability of the TiO_2 coating.

281 **Results and Discussion**

282 ***Micro Analysis Results***

283 Fig. 4a and Fig. 4b present the SEM microscopic images of L-PC and H-PC on planar
284 glass substrates. The micro features in these two images indicate that the incorporation of
285 TiO_2 nanoparticles has little impact on the porous structure (in comparison to Fig.1d).
286 Regular pores can be observed on the surfaces of both L-PC and H-PC samples. In
287 addition, it can be observed from the close-up views (insets in Fig. 4a and Fig. 4b) and
288 the cross-sectional view (Fig. 4c) that TiO_2 particles are distributed inside the pores.
289 During the BF process, the TiO_2 particles tend to coat the pore walls because of the
290 Pickering emulsions effect, which is emulsion can be stabilized by solid particles
291 adsorbed onto the interface (Binks and Lumsdon 2001).

292 To further evaluate the coating effect of BF treatment, millimeter-sized aggregate
293 particles with irregular shapes were employed as non-planar substrate. Similar to the
294 results of the TiO_2 coating on planar substrates, highly ordered porous structure can be
295 observed on most part of the aggregate surface (insets in Fig. 5a and 5b). Compared to
296 the original aggregate, honeycomb structure can be observed on the surface of aggregate
297 particles treated by the BF process. Along with the SEM images, the EDX results also
298 demonstrate the existence of titanium on the sample surfaces (Fig. 5a and 5b). Multiple
299 locations were analyzed and the EDX results from different locations indicate that

300 titanium distributed evenly on the aggregate surface. The satisfying results of TiO₂
301 coating on non-planar substrates indicate that such porous structure can also be formed on
302 pavement surface.

303 ***NO Removal Efficiency Test Results***

304 Fig. 6a presents the variations of NO concentration inside the chamber for four specimens
305 during the testing process. Each of the four curves represents one typical specimen in
306 each group shown in Table 1. As Fig. 6a shows, initially the NO concentration inside the
307 chamber was relatively constant at approximately 1200ppb. Then, after the UV lights
308 were turned on at 30 minutes, there was a rapid drop of the NO concentration for all
309 groups except for OM. A few minutes later, the second equilibrium state was reached
310 inside the chamber. At 45 minute, the UV lights were turned off and a sudden increase of
311 the NO concentration occurred.

312 Fig. 6b shows the NO removal rate of all test specimens. It can be seen that the
313 NO removal rates within each group are relatively close to each other, indicating good
314 testing repeatability. The NO removal rate of the OM specimen, which does not have any
315 coating, is almost zero. Among the three groups of specimens with TiO₂ coating, H-PCM
316 has the highest average removal rate, which is 16.4%, followed by WCM and L-PCM,
317 which have the average removal rates of 9.5% and 7.7%, respectively. It is worth noting
318 that H-PCM and WCM actually have the same amount of TiO₂ on the specimen surface,
319 which is four times of that of the L-PCM specimens. Therefore, by introducing the
320 porous structure to the coating material, much better NO removal efficiency can be
321 achieved when the same amount of TiO₂ is applied. In other words, the BF treatment

322 significantly improves the photocatalytic performance of the TiO₂ coating on the asphalt
323 mixture specimen.

324 The enhanced effect of pollution removal ability is mainly attributed to the micro
325 porous features of the coating surface. According to the mechanism of photocatalytic
326 activity, only TiO₂ particles exposed on the surface can be in contact with UV and
327 provide the catalytic effect. The micro porous structure enables TiO₂ to be distributed
328 evenly inside the micro pores, providing larger contact area among TiO₂, UV, and NO,
329 which helped accelerate the degradation of NO.

330 ***Durability Test Results***

331 Fig. 7 and Table 2 present the results of the durability tests. In Fig. 7, the columns show
332 the average NO removal rates (R%), and the curves describe the residuary NO removal
333 ability (RA%) after various numbers of abrasion. It can be seen that compared to the
334 original state, i.e., the state with no abrasion, there were obvious decreases in NO
335 removal efficiency for all test samples after 50 times of abrasion. However, there were
336 only minor drops after 200 times of abrasion, compared to after 50 times of abrasion. The
337 possible explanation is that after 50 times of abrasion, the amount and distribution of
338 TiO₂ particles on the specimen surfaces became relatively stable, leading to only slight
339 variation in the pollution removal efficiency.

340 The results also indicate that the specimens with porous coating had better
341 abrasion resistance or durability. As Fig.7 and Table 2 illustrate, H-PCM specimens had
342 an average NO removal rate of 7.92% after 200 times of abrasion, which is much higher
343 than that of WCM specimens (i.e., 2.95%). In addition, although L-PCM specimens
344 performed worse than WCM specimens in the original state, they performed better after

345 200 times of abrasion due to better abrasion resistance. The residuary NO removal
346 abilities of H-PCM and L-PCM are 47.5% and 48.3%, respectively, while that of the
347 WCM is only 31.1% after 200 times of abrasion. In other words, the porous coating
348 method provides better abrasion resistance than the traditional water-solution based
349 coating method. The enhancement of the durability can be attributed to the porous
350 structure, which protects the catalyst from direct abrasion by the rubber. Meanwhile, the
351 TiO₂ particles inside the pores are not easily be pushed inside the asphalt binder.

352 **Summary and Findings**

353 In this study, a novel coating method was proposed to incorporate the TiO₂ particles onto
354 pavement surface. This method was inspired by the BF process and Pickering emulsion
355 effect. By using this method, uniform porous structure can be fabricated on the coating
356 surface, which allows more TiO₂ to be exposed to UV lights. The photocatalytic
357 efficiency and durability of the asphalt mixture specimens coated with this new method
358 were investigated. Based on the results of this study, the following findings have been
359 obtained:

- 360 • By BF treatment, honeycomb microstructures can be introduced to asphalt
361 binder surface, and the incorporation of TiO₂ particles into asphalt binder does
362 not affect the shape of porous morphology.
- 363 • Compared to the specimens coated with the traditional water-solution based
364 method, the specimens with porous TiO₂ coating performed better in terms of
365 removing NO pollution.
- 366 • The porous coating method also provided the coating material better durability
367 to maintain the NO removal efficiency after tire abrasion.

368 With the promising findings of the laboratory testing in this study, future work
369 will be conducted to further investigate how to implement the porous coating method in
370 the field. In addition, the performance of alternative low-boiling-point solvents of asphalt
371 binder for the BF process will be studied.

372 **Acknowledgements**

373 The authors would like to acknowledge the Department of Civil and Environmental
374 Engineering of the Hong Kong Polytechnic University for funding support and the
375 technical guidance in microstructure characterization from Mr. Jianliang Gong from the
376 Institute of Textiles & Clothing of the Hong Kong Polytechnic University. The contents
377 of this study reflect the views of the authors, who are responsible for the facts and the
378 accuracy of the data presented herein. This paper does not constitute a standard,
379 specification, or regulation.

380 **References**

381 Agrios, A. G., & Pichat, P. (2005). State of the art and perspectives on materials and
382 applications of photocatalysis over TiO₂. *Journal of Applied Electrochemistry*, 35(7),
383 655-663.

384 ASTM Standard D6926. Standard Practice for Preparation of Bituminous Specimens
385 Using Marshall Apparatus, *American Society for Testing and Materials*, 2010.

386 ASTM Standard E303. Standard Test Method for Measuring Surface Frictional Properties
387 Using the British Pendulum Tester, *American Society for Testing and Materials*, 2013.

388 Atkinson, R. (2000). Atmospheric chemistry of VOCs and NO_x. *Atmospheric*
389 *Environment*, 34(12), 2063-2101.

- 390 Ballari, M. M., & Brouwers, H. J. H. (2013). Full scale demonstration of air-purifying
391 pavement. *Journal of Hazardous Materials*, 254, 406-414.
- 392 Binks, B. P., & Lumsdon, S. O. (2001). Pickering emulsions stabilized by monodisperse
393 latex particles: effects of particle size. *Langmuir*, 17(15), 4540-4547.
- 394 Bunz, U. H. F. (2006). Breath figures as a dynamic templating method for polymers and
395 nanomaterials. *Advanced Materials*, 18(8), 973-989.
- 396 Chen, M., & Liu, Y. (2010). NO_x removal from vehicle emissions by functionality
397 surface of asphalt road. *Journal of Hazardous Materials*, 174(1), 375-379.
- 398 Chen, J., & Poon, C. S. (2009). Photocatalytic construction and building materials: from
399 fundamentals to applications. *Building and Environment*, 44 (9), 1899-1906.
- 400 Dylla, H., Hassan, M. M., Thibodeaux, L. J. (2014). Kinetic Study of photocatalytic
401 degradation of emitted nitrogen monoxide using titanium dioxide nanoparticles in
402 concrete pavements, *Transportation Research Record: Journal of the Transportation*
403 *Research Board, No. 2717, CD-ROM*.
- 404 Dylla, H., Hassan, M.M., Mohanmmad, L.N., Rupnow, T., & Wright, E. (2010).
405 Evaluation of environmental effectiveness of titanium dioxide photocatalyst coating
406 for concrete pavement. *Transportation Research Record: Journal of the*
407 *Transportation Research Board*, 2164(1), 46-51.
- 408 Fujishima, A., & Honda, K. (1972). Electrochemical photolysis of water at a
409 semiconductor electrode. *Nature*, (238), 37-8.
- 410 Hassan, M. M., Dylla, H., Asadi, S., Mohammad, L. N., & Cooper, S. (2011). Laboratory
411 evaluation of environmental performance of photocatalytic titanium dioxide warm-
412 mix asphalt pavements. *Journal of Materials in Civil Engineering*, 24(5), 599-605.

- 413 Hassan, M., Mohammad, L. N., Asadi, S., Dylla, H., & Cooper III, S. (2012). Sustainable
414 photocatalytic asphalt pavements for mitigation of nitrogen oxide and sulfur dioxide
415 vehicle emissions. *Journal of Materials in Civil Engineering*, 25(3), 365-371.
- 416 Li, L., & Qian, C. (2009). A lab study of photo-catalytic oxidation and removal of
417 nitrogen oxides in vehicular emissions and its fieldwork on Nanjing No. 3 bridge of
418 Yangtze River. Technical Note. *International Journal of Pavement Research and
419 Technology*, 2(5), 218-222.
- 420 Li, L., Zhong, Y., Li, J., Gong, J., Ben, Y., Xu, J., & Ma, Z. (2010). Breath figure
421 lithography: A facile and versatile method for micro patterning. *Journal of Colloid
422 and Interface Science*, 342(1), 192-197.
- 423 Losa, M., Leandri, P., & Licitra, G. (2013). Mixture design optimization of low-noise
424 pavements. *Transportation Research Record: Journal of the Transportation Research
425 Board*, 2372(1), 25-33.
- 426 Maury-Ramirez, A., Demeestere, K., & De Belie, N. (2012). Photocatalytic activity of
427 titanium dioxide nanoparticle coatings applied on autoclaved aerated concrete: effect
428 of weathering on coating physical characteristics and gaseous toluene removal.
429 *Journal of Hazardous Materials*, 211, 218-225.
- 430 Poon, C., & Cheung, E. (2007). NO removal efficiency of photocatalytic paving blocks
431 prepared with recycled materials. *Construction and Building Materials*, 21(8), 1746-
432 1753.
- 433 Shen, S., Burton, M., Jobson, B., & Haselbach, L. (2012). Pervious concrete with
434 titanium dioxide as a photocatalyst compound for a greener urban road environment.
435 *Construction and Building Materials*, 35, 874-883.

- 436 Stempihar, J. J., Pourshams-Manzouri, T., Kaloush, K. E., & Rodezno, M. C. (2012).
437 Porous asphalt pavement temperature effects for urban heat island analysis.
438 *Transportation Research Record: Journal of the Transportation Research Board*,
439 2293(1), 123-130.
- 440 Venturini, L., & Bacchi, M. (2009). Research, design, and development of a
441 photocatalytic asphalt pavement. *Proceedings of 2nd International Conference on*
442 *Environmentally Friendly Roads: ENVIROAD*.
- 443 Widawski, G., Rawiso, M., & François, B. (1994). Self-organized honeycomb
444 morphology of star-polymer polystyrene films. *Nature*, 387-399.
- 445 Zhao, J., & Yang, X. (2003). Photocatalytic oxidation for indoor air purification: a
446 literature review. *Building and Environment*, 38(5), 645-654.
- 447

448 **List of Table Captions**

449 **Table 1.** Description of test specimens for environment test

450 **Table 2.** The mean values and standard deviation values of removal rates

451

Table 1. Description of test specimens for environment test

Group ID	Description
OM	Original Marshall specimen without TiO ₂
WCM	Marshall specimen with water-based TiO ₂ coating
L-PCM	Marshall specimen with L-PC coating
H-PCM	Marshall specimen with H-PC coating

452

453

454

Table 2. The mean values and standard deviation values of removal rates

	R ₀ %		R ₅₀ %		R ₂₀₀ %	
	Average Value	Standard Deviation	Average Value	Standard Deviation	Average Value	Standard Deviation
OM	0.093	-	-	-	-	-
WCM	9.520	0.59719	3.194	0.49487	2.956	0.54501
L-PCM	7.730	1.02587	3.737	0.27538	3.676	0.50533
HPCM	16.408	1.85565	8.517	0.46608	7.923	0.41633

455

456